Atmos. Chem. Phys., 11, 543–556, 2011
www.atmos-chem-phys.net/11/543/2011/
doi:10.5194/acp-11-543-2011

Atmospheric Chemistry and Physics

A very high-resolution (1 km × 1 km) global fossil fuel CO_2 emission inventory derived using a point source database and satellite observations of nighttime lights

T. Oda and S. Maksyutov

Center for Global Environmental Research, National Institute for Environmental Studies, Tsukuba, Japan

Received: 26 February 2010 – Published in Atmos. Chem. Phys. Discuss.: 1 July 2010
Revised: 20 December 2010 – Accepted: 4 January 2011 – Published: 18 January 2011

Abstract. Emissions of CO_2 from fossil fuel combustion are a critical quantity that must be accurately given in established flux inversion frameworks. Work with emerging satellite-based inversions requires spatiotemporally-detailed inventories that permit analysis of regional natural sources and sinks. Conventional approaches for disaggregating national emissions beyond the country and city levels based on population distribution have certain difficulties in their application. We developed a global 1 km × 1 km annual fossil fuel CO_2 emission inventory for the years 1980–2007 by combining a worldwide point source database and satellite observations of the global nightlight distribution. In addition to estimating the national emissions using global energy consumption statistics, emissions from point sources were estimated separately and were spatially allocated to exact locations indicated by the point source database. Emissions from other sources were distributed using a special nightlight dataset that had fewer saturated pixels compared with regular nightlight datasets. The resulting spatial distributions differed in several ways from those derived using conventional population-based approaches. Because of the inherent characteristics of the nightlight distribution, source regions corresponding to human settlements and land transportation were well articulated. Our distributions showed good agreement with a high-resolution inventory across the US at spatial resolutions that were adequate for regional flux inversions. The inventory can be extended to the future using updated data, and is expected to be incorporated into models for operational flux inversions that use observational data from the Japanese Greenhouse Gases Observing SATellite (GOSAT).

Correspondence to: T. Oda
(oda.tomohiro@nies.go.jp)

1 Introduction

Inventories of carbon dioxide (CO_2), which is a major greenhouse gas produced by humans, are a basic tool for monitoring compliance with the guidelines for managing national and global CO_2 emissions, and for the analysis of emission sources and trends in development. The analysis provides quantitative insights into fossil fuel CO_2 emissions and facilitates the assessment of practical measures for emission reduction, as well as informing future projections related to socioeconomic trends. Inventory monitoring of CO_2 is conducted by the US Department of Energy Carbon Dioxide Information Analysis Center (CDIAC), which maintains a continuous archive of global emission data and monitors the 20 top-emitting countries' fossil fuel CO_2 emissions (1751–2006) (e.g. Marland et al., 2008). The International Energy Agency (IEA, http://www.iea.org/) also collects national CO_2 emission data, and the statistics cover fossil fuel CO_2 emissions in more than 140 countries and regions worldwide (1971–2005), by sector and by fuel type (IEA, 2007). National inventory datasets are often available in gridded form (e.g. Andres et al., 1996; Brenkert, 1998; Olivier et al., 2005) (typically at 1° resolution) and are used as input data for physical models, such as General Circulation Models (GCMs) and atmospheric chemical transport models (CTMs), that simulate the state of atmospheric CO_2 (e.g. IPCC, 2007). CO_2 flux inversions, for example, are commonly used to quantitatively estimate surface CO_2 sources and sinks at the continental scale using a combination of atmospheric CO_2 observations and transport simulations (e.g. Gurney et al., 2002; Baker et al., 2006; Stephens et al., 2007). Flux inversions, which search for the optimal balance between sources and sinks that is consistent with observations, require a priori knowledge of fossil fuel CO_2

Published by Copernicus Publications on behalf of the European Geosciences Union.

emissions as well as a priori knowledge of biospheric exchange and oceanic fluxes. In most of the common inversion frameworks, fossil fuel emissions are assumed to be known quantities, and only biospheric and oceanic fluxes are corrected via optimization (e.g. Gurney et al., 2002). Thus, fossil fuel CO_2 emissions are important as a reference for analyzing a budget of the three fluxes (fossil fuel CO_2 emissions, and biospheric and oceanic fluxes). Gurney et al. (2005) suggested that a potential bias occurs in flux estimates obtained by flux inversions in the case that poorly articulated fossil fuel CO_2 emission estimates are used as a priori information. Beyond established flux inversions, recent studies have indicated that flux inversions may be performed at finer spatial resolution using satellite-observed CO_2 concentrations (e.g. Rayner and O'Brien, 2001; Houweling et al., 2005; Chevallier et al., 2007). Currently, several satellites monitor CO_2 levels. CO_2 concentration data are available from the Atmospheric Infrared Sounder (AIRS) satellite (e.g. Strow and Hannon, 2008), the SCanning Imaging Absorption spectroMeter for Atmospheric CartograpHY (SCIAMACHY) onboard the Environmental satellite (Envisat) (Schneising et al., 2008) and the Japanese Greenhouse Gases Observing SATellite (GOSAT) (e.g. Yokota et al., 2009; Yoshida et al., 2010), although much care is required in adapting these datasets to flux inversions (Chevallier et al., 2005). Thus, development of a spatiotemporally detailed inventory is a key requirement for emerging satellite inversion approaches.

In constructing a gridded global emission map using national emissions, the geographical distributions of emissions have been approximated using, for example, the correlation between CO_2 emissions and population density (e.g. Andres et al., 1996; Brenkert, 1998; Olivier et al., 2005). The distribution of populations is an appropriate measure of human activity at the spatial scales of countries and states (typically 1° resolution), making it theoretically useful for describing CO_2 emission distributions. Consequently, these data provide a reasonable approximation of CO_2 emissions on these spatial scales.

However, at spatial resolutions finer than the country and state levels, population statistics do not explain well the spatial characteristics of potential sources. In particular, power plants and land-based modes of transport are important sources, but are usually poorly correlated with the population distribution. In addition, population statistics cannot be used to pinpoint the exact locations of potential sources, because such data (e.g. census data) usually indicate a statistical number for a certain unit area. Thus, population statistics provide only diffuse approximations of the spatial distribution of potential source regions at fine spatial scales. Furthermore, because human settlements do not have a uniform density within a region (even in a spatial unit for statistical data collection), emissions depicted at a finer scale using population statistics may be distributed in areas where people do not actually reside, and vice verse. Recently, EC-JRC/PBL (2009) developed a global 0.1°×0.1° (10 km×10 km) spatial resolution inventory, EDGAR v4.0 (the Emission Database for Global Atmospheric Research), using geographical information such as point source locations and road networks in addition to population data.

To achieve such fine spatial resolution, satellite observations of nightlight data have been identified as being potentially useful. The nightlight data provide a global spatial distribution of the persistent lights on the Earth's surface, thereby providing a detailed map of human activities, such as human settlements, gas flares, fires, and boats that produce strong and persistent lights (mainly squid-fishing boats) (e.g. Elvidge et al., 1997). The advantage of employing nightlight distribution over the population distribution is that it indicates the exact locations and extents of human settlements. Recently, nightlight-based global CO_2 emission maps have been developed (Doll et al., 2000; Rayner et al., 2010). However, the use of nightlight data is limited by several factors. For example, the correlation between nightlight and human activity (and hence CO_2 emissions) is only strong in developed countries (e.g. Raupach et al., 2009). In addition, such data do not accurately indicate the variability in intensity of emissions from power plants and other point sources without additional information, although they do approximate well the exact locations of these sources.

For the US, these difficulties (including descriptions of temporal variations of emissions in addition to spatial patterns, which is another source of uncertainty that may significantly influence the model results) have been partially overcome by Gurney et al. (2009). The *Vulcan* project (www.purdue.edu/eas/carbon/vulcan) based its development on a fine-scale inventory (10 km×10 km) compiled by individual source sectors (Gurney et al., 2009). Furthermore, research into a more detailed fossil fuel CO_2 inventory, called *Hestia* (www.purdue.edu/climate/hestia), has been conducted for the city of Indianapolis in a pilot study. Using a combination of in situ measurements, remote sensing, and energy systems modelling, Hestia will provide a building-scale fossil fuel CO_2 inventory in near-real-time (Gurney et al., 2009). The Vulcan approach could be applied at the regional scale using the wealth of detailed information that is potentially available, but this method is difficult to apply on the global scale because of a lack of data.

In this study, we developed a global high-resolution annual emission inventory, ODIAC (Open source Data Inventory of Anthropogenic CO_2 emission), for the years 1980–2007. The primary goal of developing the ODIAC inventory is to provide a priori information on fossil fuel CO_2 emissions for regional flux inversions using GOSAT observational data. This inventory was developed by making use of a point source database and satellite nightlight data. National emissions were estimated using global fuel consumption statistics, and emissions from power plants were calculated using the point source database. Point sources were mapped to exact locations using the coordinate information available in the point source database, and the spatial distribution of the

Table 1. Summary of the national and regional annual emission estimates for the year 2006. "Code" in the second column refers to the standard country or area codes defined by the Statistical Division of the United Nations (http://unstats.un.org/unsd/methods/m49/m49.htm). National and regional emissions are shown in the national total ("total" in the third column), point source emission accompanied by the percentage of the national total ("point source" in the fourth column), and emissions from other sources ("other" in the last column). Values are reported in units of Megatonne carbon year^{-1}. ([a]: Belgium includes Luxemburg. [b]: Administrative region.)

Country name	Code	Emissions			
		Total	Point source	(%)	Other
United Arab Emirates	ARE	40.9	7.4	(17.7)	33.5
Argentina	ARG	41.7	8.7	(21.0)	33.0
Australia	AUS	109.8	61.0	(55.6)	48.8
Austria	AUT	20.2	4.4	(21.8)	15.8
Azerbaijan	AZE	9.5	2.7	(28.8)	6.8
Belgium[a]	BEL	50.4	8.2	(16.4)	42.2
Bangladesh	BGD	13.1	3.3	(24.1)	10.1
Bulgaria	BGR	13.9	6.8	(47.9)	7.4
Belarus	BLR	16.9	3.8	(22.8)	13.1
Brazil	BRA	101.1	6.5	(6.4)	94.6
Canada	CAN	171.7	46.9	(27.3)	124.8
Switzerland	CHE	12.3	0.0	(0.7)	12.3
Chile	CHL	18.3	6.5	(35.3)	11.7
China	CHN	1641.1	849.3	(51.8)	791.8
Colombia	COL	15.5	2.5	(15.1)	13.1
Czech Republic	CZE	34.9	17.4	(50.0)	17.4
Germany	DEU	242.8	116.9	(48.1)	125.9
Denmark	DNK	16.6	6.8	(41.0)	9.8
Algeria	DZA	24.0	4.6	(18.9)	19.3
Ecuador	ECU	6.5	0.8	(11.5)	6.0
Egypt	EGY	41.4	11.4	(27.5)	30.0
Spain	ESP	104.1	41.4	(39.7)	62.7
Finland	FIN	16.9	8.7	(51.9)	8.2
France	FRA	115.3	14.4	(12.6)	100.8
United Kingdom	GBR	165.4	61.9	(37.4)	103.5
Greece	GRC	28.9	13.6	(47.1)	15.3
Hong Kong[b]	HKG	21.5	0.0	(0.0)	21.5
Hungary	HUN	16.6	4.4	(26.1)	12.3
Indonesia	IDN	90.5	24.8	(27.4)	65.7
India	IND	332.4	173.8	(52.2)	158.9
Ireland	IRL	12.5	4.6	(38.4)	7.6
Iran	IRN	127.0	22.3	(17.6)	104.6
Iceland	ISL	0.8	0.0	(0.5)	0.8
Italy	ITA	134.9	45.8	(33.9)	89.1
Japan	JPN	373.6	112.8	(30.2)	260.8
Kazakhstan	KAZ	51.5	16.3	(31.6)	35.1
Republic of Korea	KOR	167.3	52.3	(31.3)	115.0
Kuwait	KWT	19.1	3.5	(18.3)	15.5
Lithuania	LTU	4.4	0.3	(7.3)	4.1
Mexico	MEX	111.2	27.8	(25.0)	83.4
Malaysia	MYS	43.9	17.7	(40.6)	25.9
Netherlands	NLD	71.7	16.6	(23.2)	55.0
Norway	NOR	11.2	0.3	(2.0)	10.9
New Zealand	NZL	10.4	2.7	(25.2)	7.9
Pakistan	PAK	36.5	6.8	(18.7)	29.7
Peru	PER	6.8	1.4	(18.2)	5.4
Philippines	PHL	18.5	9.5	(50.7)	9.3
Poland	POL	90.2	49.0	(54.5)	40.9
Portugal	PRT	18.3	6.8	(36.5)	11.7
Qatar	QAT	14.2	2.2	(14.6)	12.0
Romania	ROU	28.1	0.0	(0.0)	28.1
Russian	RUS	458.0	130.2	(28.5)	327.5
Saudi Arabia	SAU	118.8	19.3	(16.2)	99.7
Singapore	SGP	40.3	4.1	(9.8)	36.2
Slovakia	SVK	10.6	3.0	(27.2)	7.6
Sweden	SWE	16.9	0.8	(4.6)	16.1
Thailand	THA	62.9	21.0	(33.3)	42.0
Turkmenistan	TKM	14.7	1.4	(9.9)	13.1
Turkey	TUR	74.1	27.2	(37.0)	46.6
Taiwan	TWN	92.1	37.3	(40.5)	54.8
Ukraine	UKR	94.0	19.9	(21.3)	74.1
United States	USA	1746.9	765.1	(43.8)	981.7
Uzbekistan	UZB	30.5	8.4	(27.2)	22.3
Venezuela	VEN	37.9	3.3	(8.7)	34.6
South Africa	ZAF	122.6	59.4	(48.5)	63.2
North America	–	0.0	0.0	–	0.0
South and Cent. America	–	68.9	6.5	(9.6)	62.4
Europe and Eurasia	–	53.4	17.2	(32.0)	36.2
Middle East	–	89.9	21.8	(24.2)	68.1
Africa	–	76.6	15.5	(20.2)	61.3
Asia Pacific	–	66.8	7.1	(10.8)	59.7

residual emissions (total emissions minus point source emissions) was determined using the nightlight data. Because nightlight data are provided at a resolution of 30 arc seconds (approximately 1 km), CO_2 emissions can also be mapped at this resolution.

In developing this inventory, the primary focus was disaggregation of national emissions at a finer spatial scale by combining the point source database and the satellite nightlight data. In the sections that follow, we explain how the inventory was constructed and discuss its inherent limitations. Herein, the terms fossil fuel (and anthropogenic) CO_2 emissions refer to emissions over land, which are attributable to the combustion of fossil fuels (coal, oil, and natural gas). Due to the data availability, the use of an energy statistics as a data source for estimation of emissions and limitations of our method, the definition of fossil fuel CO_2 emissions in this study differs from a common definition in several ways (e.g. cement production, international bunkers and gas flares). Emissions from cement production, which are commonly included in fossil fuel CO_2 emissions, are not considered in this study. This is because data for the global spatial distributions of the emissions are not available while good emission estimates such as USGS (2010) are available. Non-land fossil fuel CO_2 emissions from sources such as international bunkers (marine and aviation) and fisheries and were included in the land emission estimates, as individual fuel consumption statistics are not available in the energy statistics we used for estimating

Table 2. Definition of geographic regions in this study. This definition was adopted from BP (2008).

Region	Definition
North America	US (excluding Puerto Rico), Canada, Mexico
South and Central America	Caribbean (including Puerto Rico), Central and South America
Europe and Eurasia	European members of the OECD plus Albania, Bosnia-Herzegovina, Bulgaria, Croatia, Cyprus, Former Yugoslav Republic of Macedonia, Gibraltar, Malta, Romania, Serbia and Montenegro, Slovenia, and Former Soviet Union (Armenia, Azerbaijan, Belarus, Estonia, Georgia, Kazakhstan Kyrgyzstan, Latvia, Lithuania, Moldova, Russian Federation, Tajikistan, Turkmenistan, Ukraine and Uzbekistan)
Middle East	Arabian Peninsula, Iran, Iraq, Israel, Jordan, Lebanon and Syria
Africa	African continent
Asia and Pacific	Brunei, Cambodia, China, China Hong Kong SAR, Indonesia, Japan, Laos, Malaysia, Mongolia, North Korea, Philippines, Singapore, South Asia (Afghanistan, Bangladesh, India, Myanmar, Nepal, Pakistan, Sri Lanka), South Korea, Taiwan, Thailand, Vietnam, Australia, New Zealand, Papua New Guinea, Oceania.

emissions. Thus, we simply kept those emissions in aggregated land emissions. Emissions from gas flares are not considered because the energy statistics do not provide the amount of gas loss attributable to gas flares and the emissions could be supplemented using exiting gas flare estimates such as estimates by the US National Oceanic and Atmosphere Administration (NOAA) (http://www.ngdc.noaa.gov/dmsp/interest/gas_flares.html). Also, the emissions that were not included herein could be introduced using supplemental existing inventories, such as USGS (2010) for cement production and EDGAR v4.0 (EC-JRC/PBL, 2009) for international bunkers, depending on users' purposes.

2 Data and methodology

Development of this inventory was performed in a stepwise manner, as discussed below. First we describe how emissions were calculated and then we describe how emissions were distributed.

2.1 National and regional CO_2 emissions

Estimates of annual national CO_2 emissions obtained in this work were based on worldwide energy statistics (2007 edition) compiled by the energy company BP p.l.c. (BP, 2008). The BP energy statistics were recently used to extend the established historical emission inventories (e.g. CDIAC) prior to updating the original inventories (e.g. Gregg et al., 2007; Myhre et al., 2009). The 2007 edition of the BP statistics, which covered the years 1965–2007, included the consumption of commercially-traded primary fuels (e.g. oil, coal, and natural gas) in 65 countries and an administrative region (see Table 1). Consumption of such fuels in six major geographical regions (North America, South and Central Americas, Europe and Eurasia, the Middle East, Africa, and Asia Pacific) was also provided to show the statistics in countries or regions that were not included in BP (2008). The definitions of geographical regions are summarized in Table 2.

Annual total CO_2 emissions for 71 regions (65 nations and an administrative region as well as the 6 major regions) were calculated from the consumption statistics for oil, coal, and natural gas. The oil statistics indicated all inland consumption, international airborne and maritime transport, and refinery fuel production and losses. Consumption of fuel ethanol and biodiesel were also included in the oil statistics. As the individual consumption of fuel ethanol and biodiesel were not provided in BP (2008), emission estimates in this study include emissions from the combustion of fuel ethanol and biodiesel, which are not included in common definition of fossil fuel CO_2 emissions. The inclusion may cause overestimation in national emission estimates compared to other studies over some countries and regions. The coal statistics in BP (2008) included the quantities of solid fossil fuels, such as bituminous coal, anthracite (hard coal), lignite, and brown (sub-bituminous) coal.

The CO_2 emissions were estimated by calculating the carbon content of the consumed fuels. Our estimation procedure paralleled the methodology specified in the revised IPCC 1996 guidelines for the national greenhouse gas inventories (IPCC, 1996), except in the estimation of national fuel consumption. The reference approach of the revised 1996 IPCC guidelines specified that the amount of total fuel supplied, which was correlated with the apparent consumption, formed the basis of calculations of national carbon supply, and the amount was calculated as the sum of the produced and imported quantities, minus the quantities attributable to international bunkers and stock changes. National emissions, as defined earlier, were calculated based on the total quantity of consumed primary fuels reported in BP (2008). The

conversion factors used in the calculation were adopted from the 2007 statistics report prepared by IEA (2007), unless specified otherwise. The quantities of nationally and regionally consumed primary fuels in BP (2008) (in million tonnes of oil equivalent per year) were first converted into energy quantities (in units of Terajoules). The quantity of natural gas in BP (2008) was given in billions of cubic meters, and a conversion factor of 0.90 was applied to express this quantity in millions of tonnes of oil equivalent (Mtoe). The obtained quantities of energy were then used to compute the carbon content of the consumed fuels. The following carbon emission factors (CFE, in tonnes of carbon per Terajoule) were applied: 15.3 (natural gas); 26.4 (coal); 20.0 (oil). The CFE adopted here for coal was calculated as the average of CFEs for anthracite, coking coal, other bituminous coal, subbituminous coal, and lignite. To account for the fraction of carbon that was not oxidized in the combustion of the fuels, correction factors of 0.99 (oil), 0.98 (coal), and 0.995 (natural gas) were applied. The annual estimates for the national/regional CO_2 emissions from primary fuel combustion were then found by multiplying the remaining carbon quantities by 44/12, which is the molecular weight ratio of CO_2 to carbon.

National and regional annual total emissions were calculated for the years 1980–2007. BP (2008) did not report quantities smaller than 0.05 (in million tonnes of oil equivalent per year) in their statistics; therefore, those quantities were assumed to be 0.05. In the estimation of annual emissions in this study, we extended emissions of the eight former Soviet Union countries (Azerbaijan, Belarus, Kazakhstan, Lithuania, Russian Federation, Turkmenistan, Ukraine, Uzbekistan) prior to the year 1991 to keep the consistency in the global emission estimates, which are the sum of 65 national and regional emissions. The consumption statistics for the eight former Soviet Union countries prior to 1985 were unavailable, and, therefore, were extrapolated by scaling to the annual total consumption for the full former Soviet Union which were provided in BP (2008).

2.2 CO_2 emissions from point sources

In addition to national and regional emissions, we separately estimated emissions from point sources using a global power-plant database. We utilized the database CARMA (Carbon Monitoring and Action, http://carma.org), which was compiled using data from national publicly disclosed databases for the US, EU, Canada, and India, and a commercial database of the world's power plants (Wheeler and Ummel, 2008). The database included emission levels and locations of over 50 000 power plants worldwide for the years 2000 and 2007, including all types of power plants (fossil fuel, nuclear, hydro, and other renewable energy plants). Data for the fossil fuel-red power plants (emission >0) with valid location information ($n=17668$) were selected from the database, and the values for the national total emissions from such power plants were calculated. Emissions of individual power plants were assigned to the locations indicated by CARMA. CARMA power plant emissions located in water grid cells were reviewed using Google Earth (http://earth.google.com/) and if the locations could not be confirmed, the emissions were included in non-point emissions.

We used data for the year 2007 to extend the emission estimation to the entire period of interest (1980–2007). The 17 668 power plants were assumed to be operational during this period, and their annual emission levels were simply scaled by the national (or regional) emission trends obtained from BP (2008). This assumption was taken because no other database to supplement power plant information such as location, intensities, commission years, operational situation (operation/maintenance, etc.) was available. In practice, the emissions for the year 2007 were used to account for the emissions for the year 2006. Emission data available in the CARMA database were derived by compiling and analyzing the data from different years, such as the eGRID database (http://www.epa.gov/cleanenergy/energy-resources/egrid/index.html); therefore, a 1-year shift in the base year did not critically affect the results.

The global spatial distribution of power plants used in this study is shown in Fig. 1. High concentrations of power plants can be seen in major emitting countries, such as the US, European countries, India, China, and Japan. In particular, power plants that generated emissions exceeding 4 MtC/yr, which were ranked as the top 100 emitting power plants in CARMA (orange-red-magenta dots in Fig. 1), were located mainly in these countries. In the Southern Hemisphere, power plants of similar size were sparsely distributed across South America, South Africa and the east coast of Australia. A scattering of relatively small power plants can be seen across Africa. By making use of the CARMA database, the spatial features of the power plant distribution for the year 2007 were directly included in our inventory.

2.3 CO_2 emissions from other sources and their spatial distribution

Emissions from power plants were estimated using the CARMA database; thus, emissions from other sources (often denoted as non-point sources) in a country (or a region) were loosely approximated by subtracting the emissions of power plants from the national (or regional) total emission distributions. The non-point sources include industrial, residential, and commercial sectors, as well as daily land transportation. Emissions from these sources could be diffuse and were not as strong or as persistent as emissions from the point sources. This approximation can be useful in globally analyzing the locations and strengths of non-point sources using a surrogate distribution. A surrogate commonly fails to distinguish point source from non-point source emissions. Both emission types are equally distributed, although point sources are

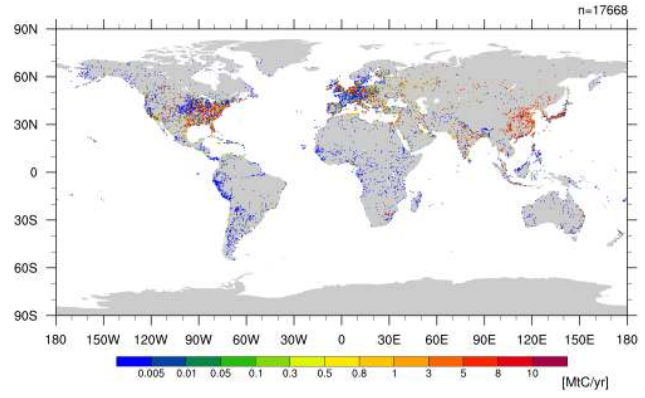

Fig. 1. Global spatial distributions of power plant emissions for the year 2007. The coordinate and emission data of power plants were taken from the CARMA database (CARbon Monitoring and Action, http://carma.org/). Power plant data with invalid coordinate information and no CO_2 emissions were excluded, and the 17 668 power plants incorporated into our inventory were plotted. Values are given in units of Megatonne carbon year^{-1}.

commonly poorly correlated with human activities. With the approximation described above, we employed a surrogate to explain only the non-point emissions.

The spatial distribution of non-point sources was determined using data from the satellite nightlight observations. The original nightlight data were obtained from the US Air Force Defence Meteorological Satellite Project Operational Linescan System (DMSP-OSL) satellites. The US National Oceanic Atmospheric Administration (NOAA) National Geophysical Data Center (NGDC) maintains the data archive, and the digital archives of standard products are available for 1997–2003. DMSP-OSL satellites are in sun-synchronous polar orbits (altitude = 830 km above the surface) and provide global coverage twice per day. The broadband visible–near infrared channel (0.4–1.1 μm), with intensification by a photomultiplier tube (PMT) in the night time, detects the clouds illuminated by moonlight as well as nightlight. Nightlight data have been used to map human settlements (Elvidge et al., 1997, 1999), gas flares (Elvidge et al., 2001), and populations (Briggs et al., 2007), as well as mapping CO_2 emissions (Doll et al., 2000; Rayner et al., 2010). It is known that intense lights such as city lights and gas flares cause instrumental saturation due to the high sensitivity of the instruments required for cloud detection. Because the radiance levels in saturated pixels are truncated, it is generally difficult to use nightlight data for mapping emissions across bright regions. Recently, Rayner et al. (2010) developed a data assimilation system for fossil fuel CO_2 emissions, FFDAS (Fossil Fuel Data Assimilation System). FFDAS is based on an extended Kaya identity, producing global emission fields by assimilating nightlights data together with other data such as population data that constrain the Kaya identity model. Rayner et al. (2010) compensated for such saturation using a correction equation derived from the probabilistic analysis presented by Raupach et al. (2009).

'radiance calibrated light' In this study, instead of correcting for saturation, the 'radiance calibrated lights' data (data available from http://www.ngdc.noaa.gov/dmsp/download_rad_cal_96-97.html) were applied as a surrogate. The 'radiance calibrated light' were obtained from special measurements acquired in a reduced-gain (low-sensitivity) mode in 1996 and 1997. This dataset has fewer saturated pixels compared with the datasets obtained by normal measurements (Elvidge et al., 1999; Cinzano et al., 2000). Cinzano et al. (2000) used the calibrated radiance data to construct a map of the night sky brightness. In this study, we utilized the correlation between the calibrated radiance data and population, which is a common surrogate as mentioned earlier. Correlation between population and the calibrated radiance data have been observed in the developed country (Elvidge et al., 1999) and we extended the relationship to whole world. The correlation however would be different over different countries and regions as previous study suggested (Raupach et al., 2009). The data have a resolution of 30 arc second (approximately 1 km) and are provided as 2-year composite data. Raw data at pixel resolution are provided in digital number (DN) format across the range 0–255, where 0 signifies that no lights were observed at a location during the observation period and 255 indicates a saturated pixel. DNs between 1 and 254 were valid and could be converted into a radiance quantity using a conversion equation. Here, we replaced DN 255 with 254 for simplicity. Consequently, emissions at pixels assigned a DN of 254 may be underestimated. As described earlier, we do not consider emissions from gas flares in this study. The pixels corresponding to gas flares were identified using a worldwide dataset of gas flares in 2004, developed by Elvidge et al. (2007), and were then eliminated.

2.4 Data integration

Annual gridded emission inventories were developed by combining emission estimates of point sources and non-point sources. Point source emissions were placed directly at exact locations using coordinate information (latitude and longitude) available in the CARMA database. National (or regional) total emissions from non-point sources were distributed to 1 km × 1 km pixels according to the distribution of nightlight radiance. The distribution was formed by superimposing the nightlight data and national boundary data, which were used to identify the national attributes of pixels. Radiance quantities across all pixels attributed to a country (or a region) were summed, and the original quantity at each pixel was normalized by the national (or regional) sum. The CO_2 emission intensity at a pixel was scaled by multiplying the normalized radiance with the annual total emission of a country or a region. We used 2.5 arc min (approximately 5 km) national boundary data (year 2000) of the Gridded Population of the World version 3 (GPWv3), developed by the

Center for International Earth Science Information Network at Columbia University, NY, USA (data available from http://sedac.ciesin.columbia.edu/gpw/global.jsp). Boundaries between land and ocean, river, and water bodies (e.g. coastline) were defined using IGBP land-cover classification data of the NASA TERRA/MODIS HDF-EOS MOD12Q1 V004 product (data available from http://duckwater.bu.edu/lc/mod12q1.html) (e.g. Belward et al., 1999). Pixels with DN of 0 (indicating water) were considered to be non-land pixels. In addition, pixels with DN of 254 (indicating unclassified) that were apparently located in ocean, river, and water bodies were included as non-land pixels.

A gridded inventory (ODIAC) for the years 1980–2007 was developed using the procedure described above. Due to the fine resolution of the nightlight data, the original ODIAC datasets for each individual year were rather large (approximately 3.5 GB). For convenience in data handling, we developed a 2.5 arc min (5 km) low-resolution inventory. The low-resolution inventory was also developed according to the method presented in this paper using 2.5 arc degree nightlight data reduced from the original 30 arc s (1 km) dataset. The analysis described in this paper was obtained from the low-resolution inventory dataset unless stated otherwise.

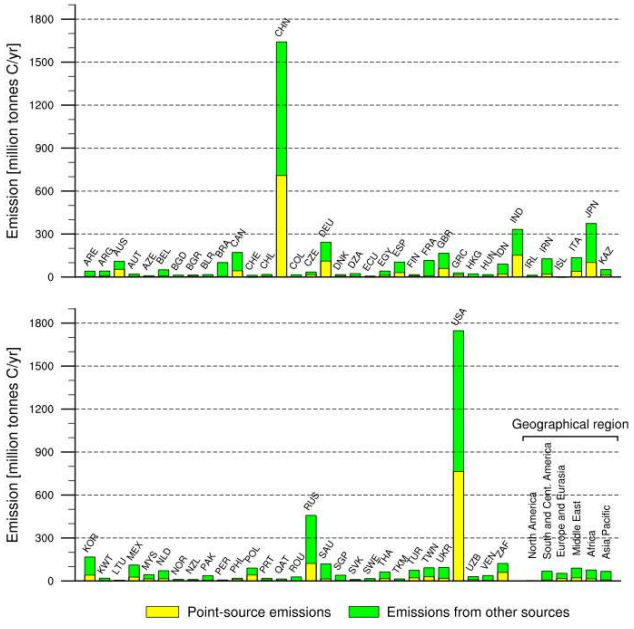

Fig. 2. National and regional total emission estimates for the year 2006. The yellow portion indicates emissions from point sources, and green indicates emissions from other sources (non-point). National and regional total point-source emissions (yellow) were calculated using the CARMA power plant data shown in Fig. 1. The non-point source emissions (green) were estimated by the residual of the total emission minus the point source emissions. Values are given in units of Megatonne carbon year^{-1}.

3 Results and discussion

3.1 Global, national, and regional annual CO_2 emissions

The estimates for national and regional annual CO_2 emissions for the year 2006 are presented in Table 1. The global total CO_2 emission for the year 2006 was estimated to be 29 992 $MtCO_2$/yr (8180 MtC/yr). In the BP-based emission estimates, the US was initially the country contributing the largest fraction of emissions (6411 $MtCO_2$/yr, equivalent to 1748 MtC/yr) and remained the world's emissions leader until the year 2007. The second-largest emitter was China (6023 $MtCO_2$/yr, 1643 MtC/yr). Other prominent emitting countries were the Russian Federation (1681 $MtCO_2$/yr, 458 MtC/yr), Japan (1371 $MtCO_2$/yr, 374 MtC/yr), and India (1220 $MtCO_2$/yr, 332 MtC/yr); these five countries accounted for 56% of the global total CO_2 emissions, according to our estimations.

The national emission levels for other countries and the fraction of point source and non-point source emissions are shown in Fig. 2. Global total CO_2 emissions from power plants were estimated to be 10 246 $MtCO_2$/yr (2794 MtC/yr), which is 34% of the global total CO_2 emission estimates in this study. Here, we note that the emissions from all power plant data available in CARMA were not summed, because invalid power plant data (e.g. zero emissions and incorrect latitude-longitude coordinate information) were eliminated at an earlier stage of the analysis. At national and regional levels, CO_2 emissions from point sources may account for a substantial proportion of the total emissions. Emissions from point sources contribute to approximately half of the total emissions in Australia (55.6%), Bulgaria (47.9%), China (51.8%), the Czech Republic (50.0%), Germany (48.1%), Finland (51.9%), Greece (47.1%), India (52.2%), the Philippines (50.7%), Poland (54.5%), and South Africa (48.5%). Because the use of just one of the common surrogates alone (e.g., nightlight or population) does not generally explain intense point source emissions, inclusion of point sources might be practical and offer a reasonable method for determining part of the spatial emission patterns. Using only one surrogate for all emissions may underestimate point source emissions and overestimate non-point sources. This may be especially important when one is interested in finer spatial scales.

As the six major geographical regions are aggregated categories of countries and regions that are not included in BP (2008), we assumed that the countries and regions within each major region had the same fraction of CO_2 emissions from point sources and non-point sources. This is a weak assumption but we did not identify a better alternative. Regardless of the weak assumption, the fraction of total emissions from point sources in the six major geographical regions (Table 1) appeared to be smaller than the fraction of emissions

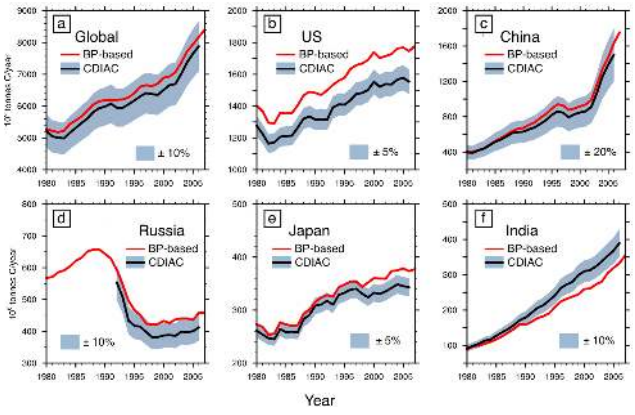

Fig. 3. Comparison of the historical global and national CO_2 emission estimates for the years 1980–2007. The red line shows the estimates given using BP (2008) in this study and black indicates CDIAC (Andres et al., 2009; Boden et al., 2009) estimates (excluding cement production and gas flaring). The shaded region shows error bounds for CDIAC taken from the literature. Values are given in units of Gigatonne carbon year^{-1}.

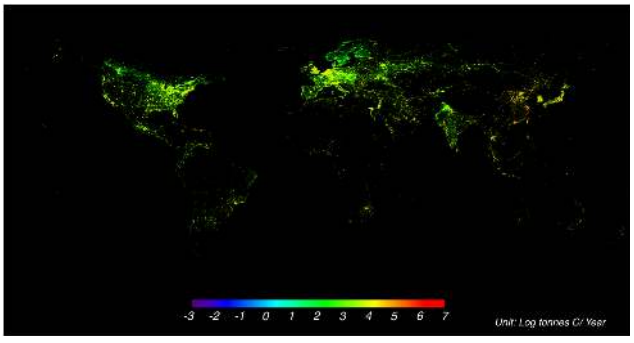

Fig. 4. Global distribution of total CO_2 emissions for the year 2006. The map was drawn using a reduced 5-km-resolution ODIAC inventory; therefore, the actual size of each pixel is 5×5 km^2. Values are given in units of the log (base 10) of tonnes carbon 5 km^{-2} year^{-1}.

from point sources in 61 countries and regions. This discrepancy may result from the fact that most industrial countries and regions were included in the 61 countries and regions. However, CO_2 emissions from point sources in the six geographical regions may still account for a considerable fraction of the total emissions.

To give a measure to the BP-based emission estimates in this study, we compared our global and national estimates with CDIAC estimates (Boden et al., 2009) (Fig. 3). The data, calculation methods, and CEFs we used differed from those in Boden et al. (2009), and thus deviations from CDIAC estimates were expected. Briefly, national total emissions from CDIAC were estimated using the apparent consumption distribution and were based on energy statistics published by the United Nations (UN, 2008) (e.g., Marland and Rotty, 1984). CDIAC global total emissions were estimated using production statistics based on (UN, 2008) (e.g. Marland and Rotty, 1984). CDIAC estimates for the comparison are the summation of emissions from the combustion of fuels (gas, liquid, and solid); emissions from cement production and gas flaring are not included. The size of error bound was taken from literature values and we would like to note that they are not always ones estimated for CDIAC emission estimates and typical values in general. We assigned 10% for global (Marland and Rotty, 1984; Marland, 2008), 5% for US (EPA, 2010) and for Japan, assuming it is a country with good statistic collection system, and 20% for China (Gregg et al., 2007). As for Russia and India, we assigned 10%, which is an error estimate for OECD countries (Olivier and Peters , 2002), assuming the two countries have the good statistic collecting system as OECD countries. We took largest numbers we found in the literatures. As shown in Fig. 3a, the global total emissions in this study overestimated CDIAC estimates. Our BP-based estimates were on average 4% higher than the CDIAC estimates in mean value, but agreed in error bounds. Comparisons of historical emission estimates for the top five emitting countries (the US, China, Russia, Japan, and India) are also shown in Fig. 3b–f. The annual national emission trends in this study agreed well with those of CDIAC, although quantitative differences between the annual emissions were present. At the national level, in particular, the deviations from CDIAC may be more apparent than at the global emission level. The calculation method in the CDIAC national estimate was based on apparent consumption, as described, whereas the national emissions in this study were derived from the annual total fuel consumption. Thus, deviations from the CDIAC estimate at the national level may be explained by, for example, the omission of adjustments for import/export and stock change and also the inclusion of international bunker emissions. Also, BP-based estimates may be higher than those of CDIAC because the BP-based includes fuel ethanol and biodiesel which CDIAC does not.

3.2 Spatial distribution of CO_2 emissions at the global, regional, and city-level scales

3.2.1 Global scale

The spatial distribution for the gridded global CO_2 emissions during the year 2006 is shown in Fig. 4. CO_2 emissions in Fig. 4 are expressed as the log (base 10) of tonnes of carbon per cell (5 km$\times$5 km) per year. Point source emissions imported from the CARMA database were directly placed in the exact locations indicated by CARMA, but this spatial distribution, which can be seen in Fig. 1, was not apparent in the global distribution, even though it was based on reduced 5-km resolution data. The most prominent features of the spatial distribution shown in Fig. 4 were dominated by non-point source emissions, which were represented in the nightlight

data. Therefore, the spatial features that were readily observable were directly inherited from the native nightlight distribution. Large concentrations of intense source areas can be seen over Eastern North America, Northern and Western European countries (e.g. UK, Belgium, and the Netherlands), and East Asian countries (e.g. India, China, South Korea, and Japan). In the Southern Hemisphere, in contrast, massive source regions are not as prevalent as in the Northern Hemisphere, as one might expect. Although individual point sources cannot be distinguished, large metropolitan areas (e.g. Los Angeles, Chicago, Mexico City, Sao Paulo, London, Paris, Moscow, Johannesburg, Delhi, Bangkok, Shanghai, Beijing, Seoul, and Tokyo) can be identified as intense sources of millions of tonnes carbon per year. In addition, we can identify regional spatial characteristics that are depicted in detail by the nightlight distribution. For example, source regions along the interstate highway network in the US, road networks around Moscow, the Trans-Siberian Railway, the Nile, and the Indus, are visible spatial characteristics even in the global picture. Those nightlights observed using DMSP-OLS instruments may not be lights attributable exactly to the sources, and may be lights coming from nearby cities. However, the distribution may still be used as a surrogate for regional unique sources, such as area sources and line sources.

As stated above, emissions at a pixel were calculated by multiplying the national (or regional) total emissions by the ratio of the radiance level at a pixel to the national (or regional) total radiance. Therefore, if the total emissions are the same, emissions at a pixel can be overestimated in a country (or region) that has a smaller number of source region pixels according to the nightlight distribution. In fact, pixels across China indicated more intense emission levels than those in the US, whereas the total national emission levels in the US in 2006 were larger than those of China in this study. This result occurs because China includes smaller source regions than does the US, if one utilizes nightlight as the unique surrogate. The same explanation may account for the differences between physically small countries that are assigned intense emission levels, such as the Netherlands, Belgium, and Japan. As seen in Fig. 4, the fine depiction of source regions could offer advantages for spatial emission mapping in countries (or regions) with physically large territories and small (or concentrated) human settlements, especially at a regional scale. Source regions indicated by population data could be diffuse due to the spatial unit used for statistical data collection, potentially resulting in the underestimation of emission intensities. Here, we assumed that the nightlight intensity was linearly and uniformly related to CO_2 emissions all over the world. The proportionality constant may actually be country-specific. Moreover, nightlight may not explain spatial variations in emissions that are attributable to differences among source sectors. Because nightlight usually correlates with human activity, it also correlates with the population distribution to a similar extent. However, the

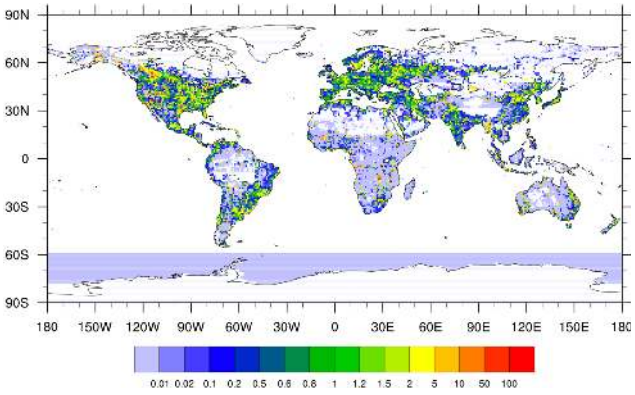

Fig. 5. The global distribution of emission ratio between our inventory (power plant data plus nightlight-based) and the CDIAC gridded inventory (population-based) for the year 2006. The emission ratio (our inventory divided by CDIAC) is calculated using our inventory (reduced to $1^\circ \times 1^\circ$ resolution from 5 km×5 km resolution) and the CDIAC $1^\circ \times 1^\circ$ gridded inventory (Andres et al., 2009). The calculated emission ratios are plotted with the range of 0.01 (1/100) and 100 (100 times). An emission ratio of 1 indicates that emissions of our inventory and CDIAC are identical, and ratios larger than 1 indicate that our inventory overestimates the CDIAC inventory, and vice versa. The regions with no color (white) indicate zero emission for both inventories. Emission pixels of our inventory with zero CDIAC emissions were not included in this analysis.

spatial distributions of nightlight and population were fairly different. As a measure of the similarities and differences, we calculated the spatial correlations and absolute differences between our inventory and the CDIAC $1^\circ \times 1^\circ$ gridded inventory for the year 2006 (Andres et al., 2009) and created a map of showing the global distribution of emission ratios between our inventory and the CDIAC gridded inventory (Fig. 5). Here, emissions of Andres et al. (2009) include emissions from cement production and fishery emissions that are not considered in this study. As the CDIAC gridded inventory was developed at a spatial resolution of 1°, the comparison was performed at the same resolution by upscaling our 5 km×5 km emission map to $1^\circ \times 1^\circ$ resolution. The emission ratios are calculated by dividing emissions in our inventory by emissions in the CDIAC inventory. An emissions ratio of 1 indicates that the emissions in our inventory and those of CDIAC are identical, and emission ratios larger than 1 indicate that our inventory overestimate the CDIAC inventory and vice versa. Emission pixels with zero CDIAC emissions (and corresponding pixels in our inventory) were not used in this analysis. The spatial correlation factor was 0.66 and the absolute difference between the two inventories was 25 332 $MtCO_2$/yr (6908 MtC/yr). The differences between the two inventories could be explained by the differences between the spatial distributions, and by emissions that were not considered in this study (see Fig. 5). As emissions from non-point sources are distributed using

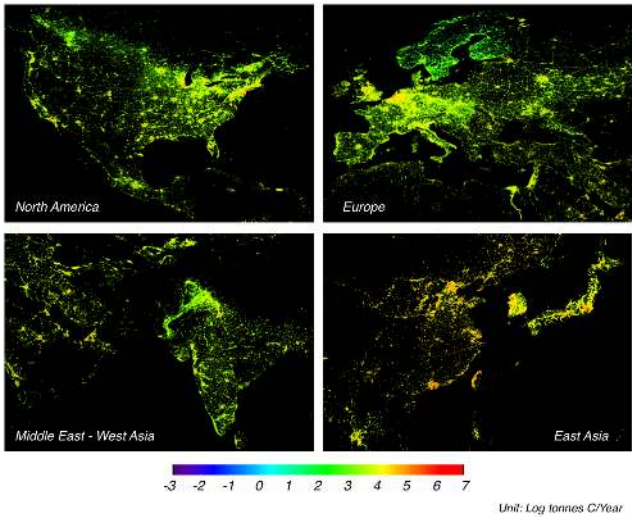

Fig. 6. Regional spatial distributions of CO_2 emissions for the year 2006. From top left (clockwise): North America, Europe, East Asia, and the Middle East and West Asia. The maps shown here were drawn using reduced 5-km-resolution ODIAC inventory on the same scale. Values are given in units of the log (base 10) of tonnes carbon $5\,km^{-2}\,year^{-1}$. Note that the maps are drawn in different scales.

the nightlight distribution, our inventory underestimated the CDIAC inventory in many places. Thus, emission ratios less than 1 can be seen at many places, especially over South America, Africa, Australia and some areas in West Asia. The underestimation over Antarctic sea is attributable to emissions from fishery, which are not considered in this study. As another feature, our inventory overestimated the CDIAC inventory at hot spots of population (populated cities and areas) and underestimated at the suburb areas (e.g., Western part of United States, South America, some parts in Europe, Africa, India and China). Our inventory often overestimated the CDIAC inventory by a factor of more than 2 at such hot spots of population.

3.2.2 Regional scale

Fig. 6 shows enlarged views of North America, Europe, East Asia, and West Asia. To determine the spatial emission patterns at the regional scale, combinations of the spatial information (e.g. industry, population, and transportation) are often used (e.g. Ohara et al., 2007; Gurney et al., 2009). In contrast, this study assumed that nightlight functioned as a comprehensive surrogate for regional sources. In fact, as shown in Fig. 4, nightlight may indicate the major transportation networks (e.g., the US and Europe) in addition to human settlements. Although individual power plants were not visible at this scale, power plants had already been placed at exact locations. The detailed regional population data may work in a similar way; however, the resultant distribution may be diffuse. It is not realistic to attempt to prepare a detailed, consistent global population map because of a lack of data.

Table 3. Comparison, across the US, of our ODIAC map and the Vulcan map. "Brenkert 1998" (the first column) is a population-based map constructed at 1° resolution (Brenkert, 1998). "FFDAS" (the second column) was based on nightlight data corrected by population data (Rayner et al., 2010). The total emissions of the participating inventories were scaled with respect to the Vulcan total emission level for the year 2002, and the sum of the absolute of the Vulcan values minus the map being compared (diff) and spatial correlations with the Vulcan map (corr) were calculated at different spatial aggregation levels (0.5°–4°) (Rayner et al., 2010). Values are given in units of Megatonne carbon.

Resolution	Brenkert 1998		FFDAS		ODIAC	
(°)	diff (MtC)	corr	diff (MtC)	corr	diff (MtC)	corr
0.5	–	–	1143	0.74	744	0.87
1.0	1045	0.75	900	0.85	474	0.94
2.0	788	0.84	651	0.91	315	0.97
3.0	654	0.87	545	0.92	262	0.98
4.0	644	0.87	479	0.93	206	0.99

A comparison of region-focused evaluations was made by comparing our ODIAC emission map with the Vulcan inventory (Gurney et al., 2009), together with the CDIAC (Brenkert, 1998) and FFDAS (Rayner et al., 2010) emission maps. The comparison was performed according to the criteria described in Rayner et al. (2010). A summary of the comparison is given in Table 3. The total emissions from the maps were scaled with respect to the Vulcan total emission level for the year 2002. The spatial correlations and absolute differences (sum of the absolute value of the Vulcan values minus the map being compared) were then calculated at different spatial scales (0.5°–4°). Among the participating maps, the CDIAC map (Brenkert, 1998) was purely population-based and has been widely used in flux inversion studies (e.g., Gurney et al., 2002). As stated earlier, FFDAS produces emission fields based on an extended Kaya identity by assimilating nightlights data together with population data. Thus, FFDAS is not solely based on nightlight data, although the contribution of nightlight data is apparent in the resulting map. The produced spatial distribution of emissions is intermediate between that of nightlight-based and population-based approaches, and is more smooth than that of traditional population-based inventories (Rayner et al., 2010). FFDAS showed better agreement with Vulcan compared with emission maps based solely on population or solely on nightlight data (Rayner et al., 2010).

The comparison results demonstrate that our emission map showed the best agreement with the Vulcan map at all spatial levels (e.g., a correlation of 0.87, even at 0.5° resolution) in terms of absolute difference and spatial pattern. Assuming that the major difference between the procedures used in FFDAS and the present study is the inclusion of point sources

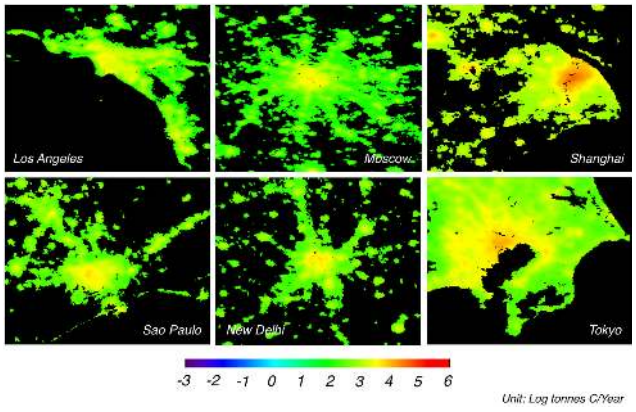

Fig. 7. Spatial distributions of CO_2 emissions over heavily populated cities worldwide for the year 2006. From top left (clockwise): Los Angeles, Moscow, Shanghai, Tokyo, New Delhi, and Sao Paulo. The maps were drawn using the original 1-km-resolution ODIAC inventory; therefore, the actual size of each pixel is $1 \times 1\,\mathrm{km}^2$. Values are given in units of the log (base 10) of tonnes carbon $1\,\mathrm{km}^{-2}\,\mathrm{year}^{-1}$. Note that the maps are drawn in different scales.

in the present study, this factor may be crucial for emission mapping at fine spatial scales. Regional agreement in spatial pattern on such spatial scales is an appealing feature for regional flux inversions, including conventional region- and grid-based types of inversions in which flux estimates are derived based on spatial patterns of a priori fluxes given as a first guess for optimization. In addition, the good quantitative agreement with the Vulcan emission maps would benefit atmospheric simulations, regardless of the fact that the comparison was performed by scaling the total emissions to the Vulcan. Here we would like note that our emission map showed better agreement with Vulcan among participant inventories as shown above, however this should not be construed to mean that the true distribution is similar to either of these distributions. The authors are aware of no independent measurements to verify any of the inventories mentioned here.

3.2.3 City-level scale

Fig. 7 shows the spatial distribution of CO_2 emissions at six major populated cities worldwide (Los Angeles, Sao Paulo, Moscow, Delhi, Shanghai, and Tokyo). Those maps were based on the native 30 arc s (1 km) resolution ODIAC inventory. As seen in Fig. 7, the local spatial structures of large cities were clearly depicted by the nightlight data. In addition, the spatial variability in CO_2 emission levels could be seen even in city cores, where standard measurements from the DMSP-OLS instruments usually register saturation. Those spatial distributions may be similar in appearance to those expected from a population-based method, and they may not explain the emission patterns by sector. Regardless of such limitations, however, the use of the 'radiance calibrated light' data enabled us to indicate possible source regions at good spatial resolution and offers a practical method for mapping emissions that can be applied to the entire globe. High-emission pixels are readily seen in Fig. 7, and some of the pixels were attributed to pixels containing power plants. Because such emitting pixels are not indicated by maps based on population or nightlight data, the individual mapping of point sources is an advantage inherent in the procedure used in this study. Because the geographical coordinates of power plants were available in CARMA, this fine-scale mapping approach fully utilized location information with reasonably small dilution. In our opinion, the available information is insufficient to fully evaluate the relationship between CO_2 emissions and nightlight intensity. In addition, we cannot evaluate the extent to which emission intensities are reasonable at this global spatial scale, as such information is only available for some individual countries, regions, or cities. Because the associated error usually increases at finer (higher) spatial resolutions, careful evaluation should be performed when utilizing the inventory presented in this study for atmospheric simulations. Regardless of such concerns, however, our high-resolution inventory may be applicable to global or regional high-resolution atmospheric simulations. In particular, one can perform, for example, atmospheric simulations with different spatial resolutions using a single consistent inventory. This inventory may also be applied toward interpreting the spatial variability in satellite CO_2 measurements globally.

3.3 Uncertainties

Here, we discuss the possible sources of uncertainties associated with our gridded emission inventory. Our procedure may include three major sources of uncertainty: (1) the calculation of national and regional emissions, (2) the use of a point source database, and (3) the use of the nightlight surrogate distribution. The first source has already been discussed in the previous section. Therefore, we will discuss the second and third sources of error.

The use of a point source database is an appealing feature of the procedure presented in this paper. To our knowledge, there are no other power plant databases publicly available that cover the entire globe. This fact was the primary motivation for utilizing the CARMA database in our development. However, CARMA obviously does not cover all existing power plants worldwide, and the emission estimate was performed using limited data (Wheeler and Ummel, 2008). In addition, geographical coordinates provided by CARMA sometimes indicate false locations. One cause of these errors is the method for deriving coordinate information. The location of power plants was generally indicated by the plants postal address in the original public data or commercial subscription data. As the postal addresses were converted into coordinate information (latitude and longitude)

via fuzzy matching using geographical information systems (Wheeler and Ummel, 2008), the addresses were sometimes erroneously assigned to places with the same name or a similar name. Assuming the locations are correct, we cannot place emissions to exact source locations if emitting points, for example boilers, are located apart from its main facility (e.g., main office mailing address). Apart from the CARMA database, we extended the CARMA emissions for the year 2007 to the years 1980–2007 using national emission trends, under the assumption that the power plants had persistently contributed emissions over the intervening years. Therefore, uncertainties may increase in the years prior to 2006, which is actually the year 2007 in the CARMA database. Considering these points, uncertainties arising from the extrapolation of emissions may be larger than those associated with selection of the base year. Total emission of CARMA power plants for the year 2000, which is the sum of year 2000 emissions from 17668 CARMA power plants used in this study, is 2138 MtC/yr and is smaller than that of year 2007 by 30% (650 MtC in emission). The difference (change in 7 years) could be explained by changes in emission intensities and power plants which are not in operation at the time. In fact, 2543 CAMRA power plants out of 17668 for 2007 (14.4%) were indicated as not operated (emission = 0) in year 2000. Our assumption does not allow us to account for both emission changes and non-operation as no data are included in CARMA and no available data to fill the gaps. Our scaled CARMA using BP trends overestimated by 8% in total emissions calculated from CARMA for 2000. With respect to the available spatial locations of power plants, we reviewed the coordinate information for 300 power plants in the CARMA data, one by one, using online resources, such as Google Earth and Wikimapia (http://wikimapia.org/). In the sample set of 300 plants, which constitutes less than 3% of the fossil fuel power plants listed in the CARMA dataset, spatial errors were often present in Chinese power plants and sometimes in Indian plants. Great care must be taken with regards to the location of power plants when using the current version of ODIAC. The next version is expected to contain the corrected locations of the 300 power plants.

The use of nightlight data is an appealing feature of the present study. We determined the spatial distribution of the source regions by assuming that nightlight directly correlates with CO_2 emissions. Whereas this assumption is applicable to developed countries, it is not well suited for developing countries (e.g., Raupach et al., 2009). Saturated pixels were assigned the highest radiance pixel values for simplicity. It was assumed that the relationship between CO_2 emissions and nightlight was linear and uniform across the different countries, although the relationship may be strongly country-dependent. In addition, we applied one composite radiance data set to all years because of the limited availability of other radiance data sets. FFDAS utilized a specific annual composite nightlight data set for each year to compile the map for that year (Rayner et al., 2010). We expect that the spatial distribution may not be significantly influenced by the employed data set, because it is not reasonable to assume that many large cities may suddenly emerge or move over the course of two decades. We do expect significant errors to arise from changes in the light intensity, which may have changed significantly, especially in developing countries and regions.

4 Conclusions

We developed a global inventory of fossil fuel CO_2 emissions (the ODIAC) for the years 1980–2007 by combining information from the global power-plant database CARMA and a special product of the DMSP-OSL satellite nightlight data. In this study, we focused on the disaggregation of national emissions using these two key components. For this purpose, we only considered land-based CO_2 emissions, which are attributable to the combustion of fossil fuels. Emissions for international bunkers, fisheries, and gas flares were not considered due to their unique emission distribution and intensities. The nightlight map was a good predictor of the spatial distribution of potential source regions up to the city level, and fossil fuel power-plant emissions were placed directly at the locations indicated in the CARMA database. The resultant spatial distribution was somewhat different from that of previously described population-based inventories. Nightlight was expected to function as a comprehensive surrogate for regional unique sources, such as population and transportation networks, beyond the features originally attributed to nightlights. Our emission map was compared with the Vulcan inventory across the US for the year 2002 and with other existing global inventories. Our inventory showed better agreement with the Vulcan inventory than did other existing inventories, with respect to spatial patterns and absolute differences, at spatial resolutions that are suitable for regional flux inversions. The comparison suggested that the inclusion of point sources may be crucial for emission mapping at fine spatial scales. Apart from flux inversions, our inventory may benefit global and regional atmospheric simulations. However, a careful quantitative evaluation may be necessary when performing atmospheric simulations using this inventory. Although it is difficult to find a single comprehensive global tool for conducting detailed global evaluations, regional evaluations may be feasible. Emerging satellite CO_2 measurements may be applicable to such evaluations. Uncertainties associated with the estimates reported in this study may arise from the calculations of national and regional emissions, the accuracy of the point source database, and the use of nightlight maps as the only surrogate emission map. These uncertainties are largely due to problems with data quality or availability, and they encompass the limitations associated with the development discussed here.

The primary motivating factor for this study was to provide a priori information on fossil fuel CO_2 emissions for flux inversions using observational data from GOSAT. We focused on fossil fuel CO_2 emissions on land. Other fossil fuel emissions that were not considered in this study, such as cement production, gas flares, international bunkers, and fisheries, may need to be accounted for by including such inventories in a full description of fossil fuel CO_2 emissions. The seasonal variations in fossil fuel emissions, as suggested in Gurney et al. (2005), may have an impact on flux estimates of inversions. In addition to annual emissions, gridded monthly emissions need to be developed for emerging monthly flux inversions. The derivation of monthly emission fields is currently under investigation.

Acknowledgements. This study was conducted as part of the GOSAT project promoted by the Japan Aerospace Exploration Agency (JAXA), the National Institute for Environmental Studies (NIES), Japan, and the Ministry of the Environment (MOE), Japan. Power plant data used in this study were taken from CARMA (CARbon Monitoring and Action, http://carma.org/). The nightlight data were obtained from US Air Force Defence Meteorological Satellite Project Operational Linescan System (DMSP-OSL) satellites processed and archived by The US National Oceanic Atmospheric Administration (NOAA) National Geophysical Data Center (NGDC). Population and national boundary data (GPWv3) were provided by the Trustees of Columbia University in the City of New York, the United Nations Food and Agriculture Programme (FAO), and the Centro Internacional deAgricultura Tropical (CIAT). The authors would like to thank Peter J. Rayner of the Laboratoire des Sciences du Climat et l'Environnement (LSCE) (now at the University of Melbourne) for his contribution to the evaluation of our product, and Stefan Reis of the University of Edinburgh for his highly useful comments on an earlier version of the manuscript of this paper. The authors also would like to thank the two anonymous referees and the editor for helping us to greatly improve the manuscript. The authors would like to acknowledge and give special thanks to Gregg Marland, T. J. Blasing and Robert J. Andres of CDIAC for their useful comments on our ODIAC development.

Edited by: C. Granier

References

Andres, R. J., Marland, G., Fung, I., and Matthews, E.: A $1^\circ \times 1^\circ$ distribution of carbon dioxide emissions from fossil fuel consumption and cement manufacture, 1950–1990, Global Biogeochem. Cy., 10, 419–429, 1996.

Andres, R. J., Boden, T. A., and Marland, G.: Annual Fossil-Fuel CO_2 Emissions: Mass of Emissions Gridded by One Degree Latitude by One Degree Longitude, doi:10.3334/CDIAC/ffe.ndp058.2009, 2009.

Baker et al.: TransCom 3 inversion intercomparison: Impact of transport model errors on the interannual variability of regional CO_2 fluxes, 1988–2003, Global Biogeochem. Cy., 20, GB1002, doi:10.1029/2004GB002439, 2006.

Belward, A. S., Estes, J. E., and Kline, K. D.: The IGBP-DIS global 1-km land-cover data set DISCover: A project overview, Photogram. Eng. Remote Sens., 65, 1013–1020, 1999.

Boden, T. A., Marland, G., and Andres, R. J.: Global, Regional, and National Fossil-Fuel CO_2 Emissions, doi:10.3334/CDIAC/00001, 2009.

BP: Statistical Review of World Energy, London, http://www.bp.com/productlanding.do?categoryId=6929&contentId=7044622, 2008.

Brenkert, A. L.: Carbon dioxide emission estimates from fossil-fuel burning, hydraulic cement production, and gas flaring for 1995 on a one degree grid cell basis, http://cdiac.esd.ornl.gov/ndps/ndp058a.html, 1998.

Briggs, D. J., Gulliver, J., Fecht, D., and Vienneau, D. M.: Dasymetric modelling of small-area population distribution using land cover and light emissions data, Remote Sens. Environ., 108, 451–466, 2007.

Chevallier, F., Engelen, R. J., and Peylin, P.: The contribution of AIRS data to the estimation of CO_2 sources and sinks, Geophys. Res. Lett., 32, L23801, doi:10.1029/2005GL024229, 2005.

Chevallier, F., Bréon, F., and Rayner, P. J.: Contribution of the Orbiting Carbon Observatory to the estimation of CO_2 sources and sinks: Theoretical study in a variational data assimilation framework, J. Geophys. Res., 112, D09307, doi:10.1029/2006JD007375, 2007.

Cinzano, P., Falchi, F., Elvidge, C. D., and Baugh, K. E.: The artificial night sky brightness mapped from DMSP Operational Linescan System measurements, Mon. Not. Roy. Astron. Soc., 318, 641–657, 2000.

Doll, C. N. H., Muller, J.-P., and Elvidge, C. D.: Night-time imagery as a tool for global mapping of socioeconomic parameters and greenhouse gas emissions, Ambio, 29, 157–162, 2000.

EC-JRC/PBL: Emission Database for Global Atmospheric Research (EDGAR), release version 4.0, http://edgar.jrc.ec.europa.eu, 2009.

Elvidge, C. D., Baugh, K. E., Kihn, E. A., Kroehl, H. W., and Davis, E. R.: Mapping city lights with nighttime data from the DSMP operational linescan system, Photogramm. Eng. Rem. S., 63, 727–734, 1997.

Elvidge, C. D., Baugh, K. E., Dietz, J. B., Bland, T., Sutton, P. C., and Kroehl, H. W.: Radiance calibration of DMSP-OLS low-Light imaging data of human settlements – a new device for portraying the Earth's surface entire, Remote Sens. Environ., 68, 77–88, 1999.

Elvidge, C. D., Imhoff, M. L., Baugh, K. E., Hobson, V. R., Nelson, I., Safran, J., Dietz, J. B., and Tuttle, B. T.: Night-time lights of the world: 1994-1995, J. Photogr. Remote Sens., 56, 81–99, 2001.

Elvidge, C. D., Baugh, K. E., Tuttle, B. T., Howard, A. T., Pack, D. W., Milesi, C., and Erwin, E. H.: A twelve year record of national and global gas flaring volumes estimated using satellite data, Final Report to the World Bank, National Oceanic and Atmosphere Administration, National Geophysical Data Center, Boulder, Colorado, USA, 2007.

EPA: Inventory of United States Greenhouse Gas Emissions and Sinks: 1990–2008, EPA 430-R-10-006, Annex 7., http://www.epa.gov/climatechange/emissions/downloads10/US-GHG-Inventory-2010-Annex-7-Uncertainty.pdf, 2010.

Gregg, J. S., Andres, R. J., and Marland, G.: China: Emissions

pattern of the world leader in CO_2 emissions from fossil fuel consumption and cement production, Geophys. Res. Lett., 35, 10288–10293, doi:10.1029/2007GL032887, 2007.

Gurney, K. R., Rachel, L. M., Denning, A. S., Rayner, P. J., Baker, D., Bousquet, P., Bruhwiler, L., Chen, Y.-H., Ciais, P., Fan, S., Fung, I. Y., Gloor, M., Heimann, M., Higuchi, K., John, J., Maki, T., Maksyutov, S., Masarie, K., Peylin, P., Prather, M., Pak, B. C., Randerson, J., Sarmiento, J., Taguchi, S., Takahashi, T., and Yuen, C.-W.: Towards robust regional estimates of CO_2 sources and sinks using atmospheric transport models, Nature, 415, 626–630, 2002.

Gurney, K. R., Chen, Y.-H., Maki, T., Kawa, S. R., Andrews, A., and Zhu, Z.: Sensitivity of atmospheric CO_2 inversions to seasonal and interannual variations in fossil fuel emissions, J. Geophys. Res., 110, D10308, doi:10.1029/2004JD005373, 2005.

Gurney, K. R., Mendoza, D. L., Zhou, Y., Fischer, M. L., Miller, C. C., Geethakumar, S., and de la Rue du Can, S.: High resolution fossil fuel combustion CO_2 emission fuxes for the united states, Environ. Sci. Technol., 5535–5541, doi:10.1021/es900806c, 2009.

Houweling, S., Hartmann, W., Aben, I., Schrijver, H., Skidmore, J., Roelofs, G.-J., and Breon, F.-M.: Evidence of systematic errors in SCIAMACHY-observed CO_2 due to aerosols, Atmos. Chem. Phys., 5, 3003–3013, doi:10.5194/acp-5-3003-2005, 2005.

IEA: CO_2 emissions from fuel combustion: 1971–2005 (2007 edition), International Energy Agency, Paris, France, 2007.

IPCC: Revised 1996 IPCC Guidelines for National Greenhouse Gas Inventories, Tech. rep., IPCC/OECD/IEA, Paris, http://www.ipcc-nggip.iges.or.jp/public/gl/invs1.html, 1996.

IPCC: Climate Change 2007: The Physical Science Basis, Cambridge University Press, Cambridge, UK, 1009 pp., 2007.

Marland, G. and Rotty, R. M.: Carbon dioxide emissions from fossil fuels: A procedure for estimation and results for 1950-82, Tellus, 36B, 232–261, 1984.

Marland, G., Boden, T. A., and Andres, R. J.: Global, Regional, and National Fossil Fuel CO_2 Emissions, In Trends: A Compendium of Data on Global Change, 2008.

Marland, G.: Uncertainties in Accounting for CO_2 From Fossil Fuels. J. of Indust. Ecol., 12, 136–139, doi:10.1111/j.1530-9290.2008.00014.x, 2008.

Myhre, G., Alterskjær, K., and Lowe, D.: A fast method for updating global fossil fuel carbon dioxide emissions, Environ. Res. Lett., 4, 034012, doi:10.1088/1748-9326/4/3/034012, 2009.

Ohara, T., Akimoto, H., Kurokawa, J., Horii, N., Yamaji, K., Yan, X., and Hayasaka, T.: An asian emission inventory of anthropogenic emission sources for the period 1980–2020, Atmos. Chem. Phys., 7, 4419–4444, doi:10.5194/acp-7-4419-2007, 2007.

Olivier, J. G. J., Aardenne, J. A. V., Dentener, F. J., Pagliari, V., Ganzeveld, L. N., and Peters, J. A. H. W.: Recent trends in global greenhouse gas emissions: Regional trends 1970–2000 and spatial distribution of key sources in 2000, J. Integr. Env. Sci., 2, 81–99, doi:10.1080/15693430500400345, 2005.

Olivier, J. G. J. and Peters, J. A. H. W.: Uncertainties in global, regional, and national emissions inventories. In Non-CO_2 greenhouse gases: Scientific understanding, control options and policy aspects, edited by: Van Ham, J., Baede, A. P. M., Guicherit, R., and WIlliams-Jacobse, J. F. G. M., Springer, New York, USA, 525–540, 2002.

Raupach, M. R., Rayner, P. J., and Page, M.: Regional variations in spatial structure of nightlights, population density and fossil-fuel CO_2 emissions, Energ. Policy, 38, 4756–4764, doi:10.1016/j.enpol.2009.08.021, 2009.

Rayner, P. J. and O'Brien, D. M.: The utility of remotely sensed CO_2 concentration data in surface source inversions, Geophys. Res. Lett., 28, 175–178, doi:10.1029/2000GL011912, 2001.

Rayner, P. J., Raupach, M. R., Paget, M., Peylin, P., and Koffi, E.: A new global gridded dataset of CO_2 emissions from fossil fuel combustion: Methodology and evaluation, J. Geophys. Res., 115, D19306, doi:10.1029/2009JD013439, 2010.

Schneising, O., Buchwitz, M., Burrows, J. P., Bovensmann, H., Reuter, M., Notholt, J., Macatangay, R., and Warneke, T.: Three years of greenhouse gas column-averaged dry air mole fractions retrieved from satellite –Part 1: Carbon dioxide, Atmos. Chem. Phys., 8, 3827–3853, doi:10.5194/acp-8-3827-2008, 2008.

Stephens, B. B., Gurney, K. R., Tans, P. P., Sweeney, C., Peters, W., Bruhwiler, L., Ciais, P., Ramonet, M., Bousquet, P., Nakazawa, T., Aoki, S., Inoue, T. M. G., Vinnichenko, N., Lloyd, J., Jordan, A., Heimann, M., Shibistova, O., Langenfelds, R. L., Steele, L. P., Francey, R. J., and Denning, A. S.: Weak northern and strong tropical land carbon uptake from vertical profiles of atmospheric CO_2, Science, 316, 1732–1735, doi:10.1126/science.1137004, 2007.

Strow, L. L. and Hannon, S. E.: A 4-year zonal climatology of lower tropospheric CO_2 derived from ocean-only Atmospheric Infrared Sounder observations, J. Geophys. Res., 113, D18302, doi:10.1029/2007JD009713, 2008.

UN: 2006 Energy Statistics Yearbook, Tech. rep., United Nations, Department for Economic and Social Information and Policy Analysis, Statistics Division, New York, USA, 616, 2008.

USGS: Minerals Yearbook – Cement, edited by: van OSS, H. G., US Geological Survey, Reston, Virginia, USA, http://minerals.usgs.gov/minerals/pubs/commodity/cement/index.html, 2010.

Wheeler, D. and Ummel, K.: Calculating CARMA: Global Estimation of CO_2 Emissions From the Power Sector, http://www.cgdev.org/files/16101_file_Calculating_CARMA_FINAL.pdf, 2008.

Yokota, T., Yoshida, Y., Eguchi, N., Ota, Y., Tanaka, T., Watanabe, H., and Maksyutov, S.: Global concentrations of CO_2 and CH_4 retrieved from GOSAT: First preliminary results, SOLA, 5, 160–163, doi:10.2151/sola.2009-041, 2009.

Yoshida, Y., Ota, Y., Eguchi, N., Kikuchi, N., Nobuta, K., Tran, H., Morino, I., and Yokota, T.: Retrieval algorithm for CO_2 and CH_4 column abundances from short-wavelength infrared spectral observations by the Greenhouse Gases Observing Satellite, Atmos. Meas. Tech. Discuss., 3, 4791–4833, doi:10.5194/amtd-3-4791-2010, 2010.